

## Atomic Scale Design and Control of Cation Distribution in Hexagonal Ferrites

Anton L. Geiler,<sup>1,2</sup> Aria Yang,<sup>1</sup> Xu Zuo,<sup>3</sup> Soack Dae Yoon,<sup>1</sup> Yajie Chen,<sup>1</sup> Vincent G. Harris,<sup>1,2</sup> and Carmine Vittoria<sup>1,2</sup>

<sup>1</sup>Center for Microwave Magnetic Materials and Integrated Circuits (CM3IC), Northeastern University, Boston, Massachusetts 02115-5000, USA

<sup>2</sup>Department of Electrical and Computer Engineering, Northeastern University, Boston, Massachusetts 02115-5000, USA

<sup>3</sup>College of Information Technical Science, Nankai University, 94 Weijin Road, Tianjin 300071, China

(Received 7 March 2008; published 5 August 2008)

Using a novel alternating target laser ablation deposition technique, Mn cations were placed in specific interstitial sites of BaFe<sub>12</sub>O<sub>19</sub> thin films as opposed to being distributed throughout the unit cell as in conventional bulk materials. The distribution of Mn cations has been confirmed experimentally and predicted theoretically. As a result of site selection, the saturation magnetization increased 12%–22%, and the Néel temperature increased by 40–60 K compared to bulk materials. This technique implies a new methodology to design and process a new generation of ferrite, oxide, and alloy materials.

DOI: [10.1103/PhysRevLett.101.067201](https://doi.org/10.1103/PhysRevLett.101.067201)

PACS numbers: 75.70.Ak, 61.05.cj, 71.45.Gm, 76.50.+g

A vast body of knowledge on the structure and the properties of ferrites has been accumulated in the past 60 years driven in part by the technological significance of these materials in diverse applications, such as permanent magnets, microwave devices, and magnetic recording media [1]. In this Letter, we propose a new approach to the deposition of epitaxial hexagonal ferrite thin films that allows the interaction between electron spins to be affected through a controlled redistribution of magnetic cations within the unit cell. The unique structure of the resulting materials is reflected in the measured changes of the magnetic properties, such as the exchange stiffness constant, saturation magnetization, Néel temperature, and ferromagnetic resonance (FMR) linewidth, with respect to materials prepared by conventional techniques. The ability to affect the magnetic properties through a controlled distribution of magnetic cations, not realizable by conventional ferrite processing techniques, suggests a new avenue to realizing new materials. Technologically, it entails the development of novel ferrites for today's demanding applications. This approach is not unique to ferrite materials and can be easily extended to other oxide, nitride, or sulfide compounds, metal alloys, and other well-ordered materials.

The BaFe<sub>12-x</sub>Mn<sub>x</sub>O<sub>19</sub> system was selected in this study for several reasons. First, Mn-substituted barium ferrites prepared by conventional ceramics methods have been thoroughly characterized and reported in the literature [2,3] providing a basis for comparison with our films. Additionally, previous studies of the BaFe<sub>12-x</sub>Mn<sub>x</sub>O<sub>19</sub> system have reported the Mn cations to be distributed among all interstitial sites in the cubic (*S*) and hexagonal (*R*) blocks of the *M*-type ferrite unit cell when prepared by conventional ceramics processing techniques [3,4]. In the following, we present experimental results and theoretical analysis that suggest selective substitution of manganese in specific interstitial sites in the *M*-type structure has been achieved in our films.

Epitaxial thin films were deposited on *c*-plane sapphire (Al<sub>2</sub>O<sub>3</sub>) substrates by alternating target laser ablation de-

position (ATLAD). A detailed description of the growth conditions has been provided elsewhere [5]. The aim of the deposition routine was to localize the Mn cations in the cubic *S* block of the hexagonal *M*-type structure. The deposition routine consisted of 3 laser pulses on the BaFe<sub>2</sub>O<sub>4</sub> target, 11 pulses on the Fe<sub>2</sub>O<sub>3</sub> target, and 11 pulses on the MnFe<sub>2</sub>O<sub>4</sub> target, concluding with another 11 pulses on the Fe<sub>2</sub>O<sub>3</sub> target deposited sequentially. As a result, 24 Å, approximately equal to the height of one unit cell ( $c = 23.17 \text{ \AA}$  [1]), were deposited per routine. As will be shown in the following sections, the placement of Mn cations in the interstitial sites of the unit cell was determined by the order in which individual targets were ablated. The deposited films were annealed at 1050 °C as previously described [6]. The proposed approach differs from the preparation of multilayer composites, where the dimensionality scale is larger and the interest is to affect the interaction between layers to introduce new electrical or magnetic properties. Our interest here is to affect local spin interactions at the atomic scale in order to induce new magnetic properties while maintaining the integrity of the unit cell.

The crystal structure of the films was studied by x-ray diffraction measurements. A representative  $\theta$ - $2\theta$  spectrum, collected using a Cu  $K\alpha$  source, is shown in Fig. 1(a). Sharp peaks corresponding to *c*-plane diffraction are clearly visible in the spectrum confirming that the films possess *c*-axis-oriented hexagonal *M*-type crystal texture. To determine the degree of epitaxy, rocking curve measurements of the highest intensity (008) diffraction peak were performed as shown in Fig. 1(b). A full width at half maximum value of 0.25° in  $\omega$  was measured suggesting that the films possess a narrow *c*-axis dispersion. The crystallographic texture of the films was analyzed by pole figure measurements using a general area detector and is shown in Fig. 1(c). Sixfold symmetry was observed in the (107) diffraction peaks indicating that the films possess a high degree of in-plane orientation.

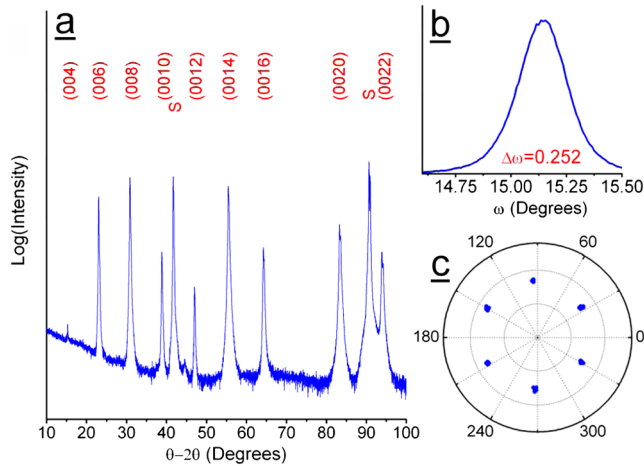


FIG. 1 (color online). Sample  $\theta$ - $2\theta$  x-ray diffraction spectrum (a). Rocking curve measurement of the highest intensity (008) diffraction peak (b) and pole figure measurement of the (107) diffraction peak (c).

Extended x-ray absorption fine structure (EXAFS) analysis was utilized to determine the distribution of Mn cations among the interstitial sites of the hexagonal unit cell. Mn  $K$  edge absorption data were collected at the X23B beam line of the National Synchrotron Light Source from 200 eV below to 12 photoelectron wave numbers ( $k$ ) above the absorption edge. The truncation at  $12k$  was due to the onset of the Fe  $K$  edge at 7112 eV. The EXAFS data were fit to theoretical standards generated by FEFF version 6 [7] and analyzed using the software codes of ATHENA and ARTEMIS [8]. Cation distribution information was retrieved from the best fit following the approach previously established for spinel ferrites [9–11]. The best fit EXAFS data are presented with the experimental Mn  $K$  edge EXAFS in Fig. 2(a) in photoelectron wave vector space (i.e.,  $k$ , with  $k^2$  weighting) and Fig. 2(b) as the real part of the Fourier-transformed EXAFS data. The quality of the best fit in Fig. 2 is reflected by an  $R$  factor of 0.04. These fitted data were optimized over a range of radial coordinates from 1 to 6 Å [ $k$  range of 2–10 Å<sup>-1</sup> for Fig. 2(a)]. The fitting model included 89 photoelectron scattering paths and multiple scattering paths leading to the determination of the Mn occupancy among the five inequivalent sites of the magnetoplumbite structure. In this unit cell, 2.3(2) Mn ions were measured to occupy the octahedral  $12k$  sites at the interface between  $S$  and  $R$  blocks, while 0.7(2) Mn ions were found to reside on the tetrahedral  $4f_{IV}$  sites of the  $S$  block. The location of these sites in the unit cell is shown in Fig. 3(a). No Mn ions were measured to reside on other unit cell sites within the uncertainty of the fitting analysis. Average Mn-O bonding distances for the  $4f_{IV}$  and  $12k$  sites were determined from the best fit to be 1.92(7) and 1.94(7), respectively.

X-ray absorption near edge fine structure analysis was carried out from 30 eV below to 50 eV above the absorption

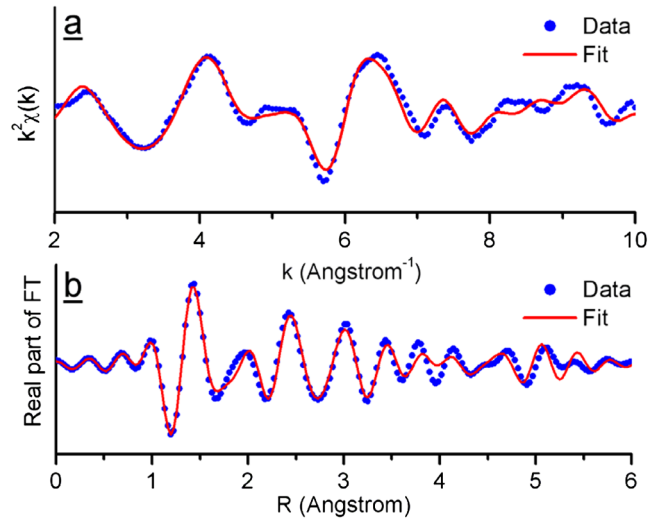


FIG. 2 (color online). EXAFS data with the best fit from the Mn  $K$ -edge absorption in photoelectron wave vector space (a). Real part of the Fourier transform (FT) of the EXAFS data with the best fit from the Mn  $K$ -edge absorption (b).

edge (not shown). The near edge spectra are strongly influenced by x-ray-induced transitions of the core electrons to unoccupied energy levels and are therefore very sensitive to the electronic structure of the absorbing ions. Linear combination fits of the data from the Fe and Mn oxide powder standards resulted in an average valence state of +2.82 for Mn and +2.98 for Fe.

Based on the observed number of Mn and Fe cations in the unit cell, the average composition of the films corresponded to a bulk composition of BaFe<sub>10.5</sub>Mn<sub>1.5</sub>O<sub>19</sub>. However, according to the EXAFS results presented above, the cation distribution in the films was principally different

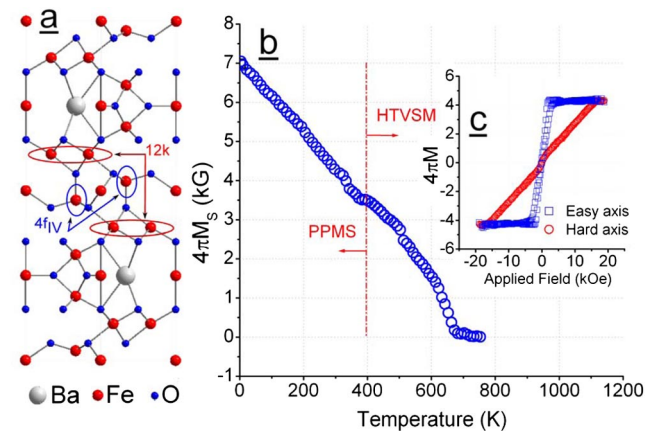


FIG. 3 (color online). Unit cell of hexagonal  $M$ -type barium ferrite (a). Magnetization as a function of temperature measured by the Quantum Design PPMS 4–300 K and high temperature vibrating sample magnetometer attachment (HTVSM) 300–850 K (b). Room temperature hysteresis loops with the external field applied perpendicular (easy) and parallel (hard) to the film plane (c).

from that previously reported in the literature for bulk material. As opposed to being distributed among the various interstitial sites in the  $R$  and  $S$  blocks [3,4], the Mn cations are predominantly concentrated in the octahedral  $12k$  sites at the interface of  $S$  and  $R$  blocks and tetrahedral  $4f_{IV}$  sites within the  $S$  block, as was intended in the design of the deposition routine.

To validate the observed cation distribution theoretically, the total energy and the relaxed ionic positions within the Mn-substituted barium ferrite were calculated using *ab initio* methods. The calculations were performed using the generalized gradient approximation (GGA) exchange correlation [12] and the ultrasoft pseudopotential [13] methods. Both ionic positions and lattice parameters were relaxed using the conjugate gradient method. A  $4 \times 4 \times 1$   $k$  mesh in the inverse space was utilized. The break conditions for the electronic and ionic loops were  $1 \times 10^{-4}$  and  $1 \times 10^{-3}$  eV, respectively. The calculations were performed using the VIENNA AB INITIO SIMULATION PACKAGE [14]. Total energies of unit cells with 2 Mn cations occupying various interstitial sites in the cubic  $S$  block were computed. The configuration with Mn cations occupying  $4f_{IV}$  sites only was taken as a reference. The lowest energy ( $-0.6$  eV) was obtained when Mn cations occupied nearest neighbor  $4f_{IV}$  and  $12k$  sites where the relaxation of the Mn-occupied  $4f_{IV}$  site to a lower symmetry was observed. Average Mn-O bonding distances for the  $4f_{IV}$  and  $12k$  sites were calculated to be 1.927 and 1.923 Å, respectively. The cation distribution and the local structure determined experimentally by EXAFS are thus in good agreement with the theoretical predictions of the *ab initio* calculations. The magnetic moment in the  $4f_{IV}$ - $12k$  configuration was calculated using GGA to be about 4% higher than that of intrinsic barium ferrite.

Room temperature magnetization measurements were carried out by vibrating sample magnetometry. Typical hysteresis loops are shown in Fig. 3(c). The small coercive fields determined from the hysteresis loop measurements with the external field applied perpendicular to the film plane were indicative of the high crystalline quality of the films. The magnetocrystalline anisotropy coefficients were consistent with the reference data on intrinsic barium ferrite [1]. Therefore, the contribution to the magnetocrystalline anisotropy of the substituted Mn ions is similar to that of  $Fe^{3+}$  ions. A high temperature furnace attachment allowed measurement of magnetization as a function of

temperature up to 850 K. Low temperature magnetization measurements to 4 K were carried out using a Quantum Design physical property measurement system (PPMS). Magnetizations as a function of temperature curves obtained by the above methods are superimposed and presented in Fig. 3(b). Several measured magnetic properties of the films are summarized in Table I and compared to the properties of bulk  $BaFe_{10.5}Mn_{1.5}O_{19}$  deduced from a linear interpolation of the reference data [2]. The values of low temperature saturation magnetization of the films were approximately 12%–22% higher than that of bulk Mn-substituted barium ferrite. Room temperature magnetization was approximately 5%–15% higher, and the Néel temperature was about 40–60 K higher. The low temperature saturation magnetization of the films was consistent with that of intrinsic barium ferrite [1] and in good agreement with the predictions of the *ab initio* calculations.

The observed increase of 40–60 K in the Néel temperature, as well as the 12%–22% increase in the saturation magnetization over the bulk Mn-substituted barium ferrite value [2], stem from the discrete distribution of Mn cations among only  $12k$  and  $4f_{IV}$  sites. As a result, fewer exchange interactions are weakened by the presence of  $Mn^{3+}$ . The weakening of exchange interactions as a function of  $Mn^{3+}$  substitution is evidenced by the lower Néel temperature compared to intrinsic barium ferrite films [5], as well as exchange stiffness constant measurements to be discussed shortly. In fact, the dominant exchange interaction between  $4e(\frac{1}{2})$  and  $4f_{VI}$  sites, largely responsible for the net ferromagnetic moment, would remain mostly unaffected as a result of the observed  $Mn^{3+}$  distribution.

FMR measurements were carried out by the shorted waveguide method in the 40–60 GHz frequency range with the films attached to the waveguide wall in an external magnetic field applied perpendicular to the film plane. In this configuration, the FMR condition is given by Eq. (1) [15]

$$\omega = \gamma \left[ H_n + H_A - 4\pi M_S + \frac{2A}{M_S} \left( \frac{\pi}{t} \right)^2 n^2 \right], \quad (1)$$

where  $\gamma = -ge/2m_e$  is the electron gyromagnetic ratio,  $H_n$  is the  $n$ th spin-wave mode resonance field,  $H_A$  is the uniaxial magnetocrystalline anisotropy field,  $M_S$  is the saturation magnetization,  $A$  is the exchange stiffness constant, and  $t$  is the thickness of the film. Resonance frequencies of the uniform mode and spin-wave resonance modes

TABLE I. Comparison of the magnetic properties of  $BaFe_{10.5}Mn_{1.5}O_{19}$  bulk and films.

	$M_S$ (4 K) ( $\mu_B$ per f.u. <sup>a</sup> )	$M_S$ (300 K) ( $\mu_B$ per f.u.)	$H_A$ (300 K) (kOe)	$K_1$ (300 K) ( $10^6$ erg/cm <sup>3</sup> )	$H_{C, \text{easy}}$ (300 K) (kOe)	$T_N$
Bulk <sup>b</sup>	18.0	11.7	16.9	2.7	...	630
Film	21.1(9)	12.9(6)	17.0(2)	2.9(2)	0.15(5)	683(10)

<sup>a</sup>f.u. denotes formula unit.

<sup>b</sup>Estimated for the  $BaFe_{10.5}Mn_{1.5}O_{19}$  composition from Ref. [3].

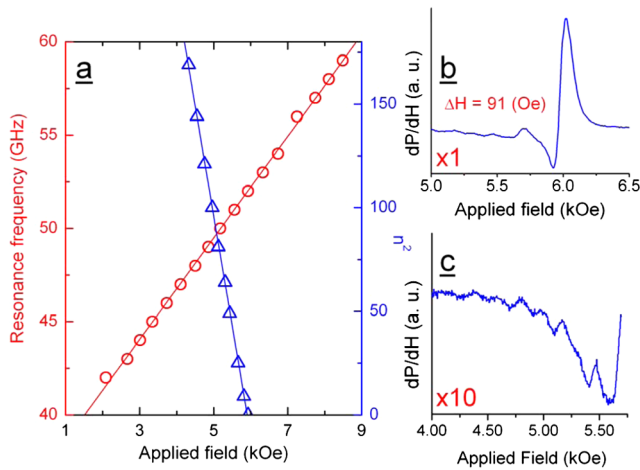


FIG. 4 (color online). Ferromagnetic resonance frequency and spin-wave resonance mode index squared as a function of applied field (a). Main resonance line ( $\times 1$ ) (b) and spin-wave resonance manifold ( $\times 10$ ) (c) at 52 GHz.

are plotted in Fig. 4. From the FMR data, a  $g$  factor of 1.96,  $A$  of  $4.1(2) \times 10^{-7}$  erg/cm, and narrowest peak-to-peak linewidth of 91 Oe were deduced following a previously outlined approach [5].

The cation distribution analysis carried out on the deposited films has shown that, unlike in previously published studies, selective cation substitution at the atomic scale has been achieved by the ATLAD technique. As a result, the interaction between local spins was fundamentally modified through a controlled redistribution of magnetic cations within the unit cell. The increases in magnetic moment and Néel temperature compared to bulk material were related to the differences in specific interstitial site occupation by Mn ions in the  $S$  block of the unit cell. In a similar fashion, the magnetocrystalline anisotropy of hexagonal ferrites could be affected by channeling proper cations to the  $R$  block of the unit cell. We believe that the long sought capability of controlling the cation distribution in ferrites, unattainable by conventional processing methods, has been realized by the ATLAD technique. This approach may usher in the design and processing of a new generation of ferrite materials and also be easily extended to other oxide, sulfide, or nitride compounds, metal alloys, and other well-ordered materials.

This research was supported by the U.S. Office of Naval Research under Grant No. N00014-05-1-0349 and the National Science Foundation under Grant No. DMR-0400676. X.Z. gratefully acknowledges the support of the China National Science Foundation under Grant

No. 60601001 and the Ministry of Education under Grant No. NCET-06-0219. This research, in part, was performed at the National Synchrotron Light Source (Brookhaven National Laboratory, Upton, NY), which is sponsored by the U.S. Department of Energy. This work made use of the MRSEC Shared Experimental Facilities at MIT, supported by the U.S. National Science Foundation under Grant No. DMR-0213282. Dr. Scott Speakman is gratefully acknowledged for his assistance with x-ray diffraction measurements. The authors thank Professor Werner P. Wolf for valuable suggestions during the preparation of the manuscript.

- [1] H. Kojima, *Ferromagnetic Materials*, edited by E.P. Wohlfarth (North-Holland, Amsterdam, 1982), Vol. 3, pp. 305–391.
- [2] X. Obradors, A. Collomb, M. Pernet, J.C. Joubert, and A. Isalgué, *J. Magn. Magn. Mater.* **44**, 118 (1984).
- [3] A. Collomb, X. Obradors, A. Isalgué, and D. Fruchart, *J. Magn. Magn. Mater.* **69**, 317 (1987).
- [4] P. Sharma, R. A. Rocha, S. N. Medeiros, B. Hallouche, and A. Paesano, Jr., *J. Magn. Magn. Mater.* **316**, 29 (2007).
- [5] A. L. Geiler, S. D. Yoon, Y. Chen, C. N. Chinnasamy, Z. Chen, M. Geiler, V. G. Harris, and C. Vittoria, *Appl. Phys. Lett.* **91**, 162510 (2007).
- [6] A. L. Geiler, S. D. Yoon, Y. Chen, A. Yang, C. N. Chinnasamy, M. Geiler, V. G. Harris, and C. Vittoria, *J. Appl. Phys.* **103**, 07B914 (2008).
- [7] J. J. Rehr and R. C. Albers, *Rev. Mod. Phys.* **72**, 621 (2000).
- [8] B. Ravel and M. Newville, *J. Synchrotron Radiat.* **12**, 537 (2005).
- [9] V. G. Harris, N. C. Koon, C. M. Williams, Q. Zhang, M. Abe, and J. P. Kirkland, *Appl. Phys. Lett.* **68**, 2082 (1996).
- [10] S. Calvin, E. E. Carpenter, V. G. Harris, and S. A. Morrison, *Appl. Phys. Lett.* **81**, 3828 (2002).
- [11] S. Calvin, E. E. Carpenter, B. Ravel, V. G. Harris, and S. A. Morrison, *Phys. Rev. B* **66**, 224405 (2002).
- [12] J. P. Perdew, J. A. Chevary, S. H. Vosko, K. A. Jackson, M. R. Pederson, D. J. Singh, and C. Fiolhais, *Phys. Rev. B* **46**, 6671 (1992).
- [13] G. Kresse and J. Furthmuller, *Phys. Rev. B* **54**, 11169 (1996).
- [14] G. Kresse and J. Furthmuller, “VASP the GUIDE,” Institut für Materialphysik, Universität Wien, Sensengasse 8, A-1130 Wien, Austria (<http://cms.mpi.univie.ac.at/vasp/vasp.pdf>).
- [15] C. Vittoria, *Microwave Properties of Magnetic Films* (World Scientific, Singapore, 1993), pp. 69–102.